Thin Solid Films 520 (2012) 1734–1739

Contents lists available at SciVerse ScienceDirect

Thin Solid Films

journal homepage: www.elsevier.com/locate/tsf

Structural and electrical properties of $LuMnO_3$ thin film prepared by chemical solution method

Y. Romaguera-Barcelay [a,b], J. Agostinho Moreira [b], A. Almeida [b], J. Pérez de la Cruz [a,*]

[a] INESCPorto, Rua do Campo Alegre, 687, 4169-007, Porto, Portugal
[b] IFIMUP and IN—Institute of Nanoscience and Nanotechnology, Departamento de Física da Faculdade de Ciências da Universidade do Porto. Rua do Campo Alegre, 687, 4169-007 Porto, Portugal

ARTICLE INFO

Article history:
Received 3 February 2011
Received in revised form 10 August 2011
Accepted 11 August 2011
Available online 30 August 2011

Keywords:
Multiferroics
Manganites
Thin films
Sol–gel deposition
Magnetic properties

ABSTRACT

Hexagonal $LuMnO_3$ thin films have been prepared based on a chemical solution deposition method. These films were deposited by spin-coating technique and annealed at different temperatures from 750 °C up to 850 °C, based on the thermogravimetric and differential thermal analysis results. An amorphous phase is observed in the film annealed at 750 °C, while a pure $LuMnO_3$ hexagonal phase is reached in the films annealed at 800 °C and 850 °C, along with a visible enhancement in the grain morphology as the annealing temperature increase. Low temperature magnetic analysis of the $LuMnO_3$ films annealed at 850 °C reveals several magnetic transitions, which are consistent with those reported for both $LuMnO_3$ ceramics and single crystals. Moreover, the emergence of a canted spin arrangement was evidenced from the temperature dependence of the specific induced magnetization and magnetic hysteretic cycles. No significant effect of the substrate on the magnetic properties was also sorted out. Dielectric measurements reveal the existence of a complex frequency behavior of the dielectric permittivity, which can be associated with relaxation processes arising from the interfaces film/electrodes.

© 2011 Elsevier B.V. All rights reserved.

1. Introduction

In the last decade, a considerable interest in yttrium, bismuth and rare-earth manganese oxides has emerged, mainly due to the fundamental issues involved, like the colossal magnetoresistance effect [1], and to their applications in advanced technology, like the application in non-volatile memory devices [2] and ferroelectric gates [3]. These materials crystallize mainly in two types of structures: orthorhombic and hexagonal. The type of structure achieved is strongly dependent on the radius of yttrium, bismuth or the rare-earth ions. A distorted perovskite-type orthorhombic structure with a space group *Pbnm* was reported for bismuth ($BiMnO_3$) [4] and larger rare-earth ions, such as: dysprosium ($DyMnO_3$) [5], gadolinium ($GdMnO_3$) [5], europium ($EuMnO_3$) [6], lanthanum ($LaMnO_3$) [4] manganites. Contrarily, a non-centrosymmetric hexagonal structure with a space group $P6_3cm$ was reported at room temperature for yttrium ($YMnO_3$) [7,8] and smaller rare-earth ions, such as: ytterbium ($YbMnO_3$) [9,10] and holmium ($HoMnO_3$) manganites [11].

The hexagonal structure consists of close-packed layers of bipyramidal MnO_5 sites sharing corners in the (001) planes. In this structure, the cooperative tilting of the bipyramidal sites displaces the cations (Ho-Lu, Y, Sc) along the *c* axis, making the compounds ferroelectric [12]. Meanwhile, the antiferromagnetic coupling between the spins of the close-packed Mn^{3+} ions of an (001) plane is frustrated, resulting in a significantly lower spin-ordering temperature [11]. It is well known that hexagonal structured materials show ferroelectric properties with fairly large remanent polarization and quite high Curie temperature (T_C), typically above 590 K. Furthermore, they exhibit an antiferromagnetic phase with a Néel temperature (T_N) in the range of 70 K–120 K, associated with geometrical frustration [5]. Both ferroelectric and antiferromagnetic orders are still coupled at low temperatures, turning the hexagonal manganites members of that set of materials that exhibit magnetoelectric effect. The existence of this effect provides the prospect of manipulating electrical properties through magnetic fields and vice versa [11,13,14].

Based on the aforementioned features, a lot of attention has been drawn on ceramic and single crystal of hexagonal manganites, which have been processed by several methods and thoroughly characterized by a set of diverse techniques [4,11,15,16]. However, the study of these materials in thin film form is rather scarce.

In this work, we report the processing procedure of $LuMnO_3$ thin films by chemical solution method and a detailed analysis of their structure, microstructure and surface morphology. Moreover, in order to determine the magnetic and dielectric response of the films, both the specific induced magnetization and dielectric permittivity were studied, as a function of the temperature, from 5 K up to 300 K. The experimental results were analyzed with comprehensive models, and further compared with those previously reported for single crystals and ceramics.

* Corresponding author.
E-mail address: jcruz@inescporto.pt (J.P. de la Cruz).

0040-6090/$ – see front matter © 2011 Elsevier B.V. All rights reserved.
doi:10.1016/j.tsf.2011.08.044

2. Experimental procedure

2.1. Precursor solution and films preparation

$LuMnO_3$ precursor solution was prepared starting from lutetium (III) nitrate hydrate that was 99.99% pure (supplied by *Aldrich*), which was previously dissolved at 50 °C in a 2:1 glacial acetic acid and nitric acid molar ratio, for 24 h. Once the lutetium precursor solution was obtained, a stoichiometric molar content of manganese (II) acetate tetrahydrate that was 99.99% pure (supplied by *Merck*) was added to it. The resulting solution was stabilized with pure 2-methoxyethanol, in a solvent (2:1:6) molar ratio, until a final 0.2 molar concentration.

Lutetium manganite precursor solution was deposited onto Pt (111)/Ti/SiO_2/Si substrates, using a Laurell WS-400-6NPP automatic spin-coater. Each individual layer was deposited at 3000 rpm for 60 s, dried at 80 °C in a hot-plate for a minute and pre-sintered at 400 °C in a tubular furnace for 10 min. This process was repeated 5 times in order to obtain multilayer films with ~250 nm. Finally, the resulting pre-sintered films were annealed at 750 °C, 800 °C and 850 °C for an hour, followed by a quenching at 25 °C in air atmosphere. In order to simplify the comprehending of the text, we called the films annealed at 750 °C, 800 °C and 850 °C as: $LuMnO_3$-A, $LuMnO_3$-B and $LuMnO_3$-C, respectively.

2.2. Experimental characterization techniques

Thermogravimetric (TG) and differential thermogravimetric analyses (DTA) were carried out in the $LuMnO_3$ solution, using a Seteram Labsys TG–DTA/DSC analyzer. In order to perform the TG and DTA measurements, the solution was previously dried at 100 °C for 48 h, forming the so-called *dry* solution. Afterwards, it was heated in air atmosphere at a rate of 10 °C/min from room temperature up to 1000 °C.

Grazing angle X-ray diffraction patterns of the films were recorded by a Phillips diffractometer equipped with copper Kα radiation (1.5418 Å). The measurements were performed in step mode at 0.01°/10 s from 20° to 80° (2θ).

Scanning electron microscopy (SEM) images were recorded by Jeol field emission scanning electron microscope, working at 15 kV at 11 mA, while the elemental composition of the films was determined using an energy dispersive X-ray analyzer attached to the microscope. The surface morphology of the films was analyzed by atomic force microscopy (AFM) technique, using a Veeco Multimode NanoScope IVa, working in tapping mode.

In order to carry out the dielectric characterization of the films, aluminum electrodes 1 mm in diameter and 100 nm thick, were deposited on the top of the $LuMnO_3$ films by evaporation technique. The dielectric measurements, carried out using a driving voltage of 0.1 V at 1 kHz, 10 kHz, 100 kHz, 600 kHz and 1 MHz, were performed in heating run from 5 K up to room temperature by using a close-cycle cryostat system and a Hewlett-Packard precision LCR E4090A meter, controlled by a LabView® program.

The magnetic properties were measured using a Quantum Design commercial superconducting quantum interference magnetometer, model MPMS-S. After previous cooling down to 5 K under zero (zero field cooled—ZFC) and 10 mT applied magnetic field (field cooled—FC), the measurements were carried out in heating run from 5 K–300 K using a driving magnetic field of 10 mT. Magnetic hysteresis loops ($M(H)$) were measured at different temperatures using a maximum applied magnetic field of 5 T and a driving a.c. magnetic field of 10 mT.

3. Results and discussion

3.1. Solution analysis

Fig. 1 shows the TG–DTA curves of the $LuMnO_3$ precursor solution. The *dry* solution decomposition process includes three main steps,

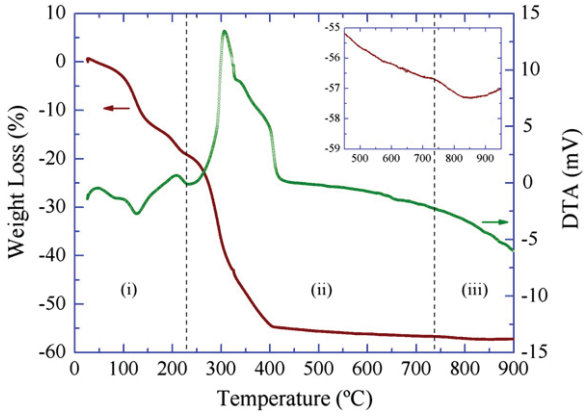

Fig. 1. Thermal decomposition curves of the $LuMnO_3$ solution. The inset plot shows the phase formation temperature region.

similar to those reported for $LaMnO_3$, $EuMnO_3$ and $DyMnO_3$ films [17]. In the evaporation step (*i*), the weight loss associated with the solvent and constitutional water evaporation is approximately 17%, in good correlation with the DTA endothermic peaks. The second step (*ii*) is characterized by a huge weight loss (~40%), associated with the decomposition of the organic materials into carbonates, which takes place in the 230 °C–400 °C temperature range. This carbonated formation is in agreement with the wide DTA endothermic peak observed around 330 °C [18]. The organic cation carbonization can be considered as the major competition reaction during the organic material decomposition, due to the oxidation of the organic compounds in air [18]. Minor weight loss (~5%) occurs still in step (*ii*) within the 400 °C–740 °C temperature range, which can be associated with the decomposition of some carbonate species into lutetium and manganese oxy-carbonates. The third and final step (*iii*) takes place above 740 °C, showing a weight loss of ~1% relatively to the initial weight of the *dry* solutions. Although the TG–DTA steps, temperature intervals, and curves profiles obtained during the decomposition of the solutions depend on the chemical element used (Y, Bi or rare-earth) [17,18], their trends are similar. The behavior in the decomposition referred to above apparently suggests the formation of a $LuMnO_3$ crystalline phase in the 740 °C–810 °C temperature range (see inset plot of Fig. 1).

3.2. Structural characterization

Fig. 2 shows the grazing angle X-ray diffraction patterns of the as-prepared $LuMnO_3$-A, $LuMnO_3$-B and $LuMnO_3$-C films, respectively. X-ray diffraction pattern of the $LuMnO_3$-A film reveals an amorphous phase overlapped with the substrate diffraction peaks, while the $LuMnO_3$-B film shows an incipient crystalline phase formation, characterized by the presence of the (002), (004) and (112) peaks. Conversely, the pattern obtained for the $LuMnO_3$-C film shows a well-defined peak structure, which is characteristic of a pure polycrystalline phase. The diffraction peaks, excluding those coming out from the substrate, were assigned to a pure hexagonal structure with a preferential (002) orientation and a space group $P6_3cm$ [15,16]. The lattice parameters obtained for the $LuMnO_3$-C film ($a = 6.006(9)$ Å and $c = 11.369(6)$ Å) are in reasonable agreement with those previously reported for the hexagonal $LuMnO_3$ ceramic [16] and single crystal [15], as shown in Table 1.

A representative SEM cross-section image of all the films is shown in Fig. 3a), where a common thickness of 260 nm was determined. It is important to note that the image, recorded on the $LuMnO_3$-C film, is also suitable for the other two analyzed films. Fig. 3b) shows the energy dispersive X-ray spectroscopy (EDS) analysis for this film. It exhibits peaks corresponding to the $LuMnO_3$ film, the carbon paste used in the SEM analysis, and the silicon, titanium, and platinum

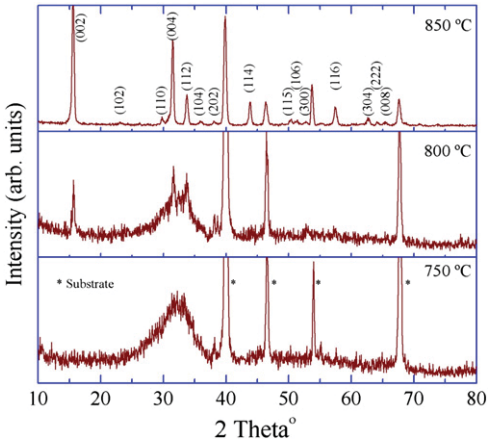

Fig. 2. Grazing angle X-ray diffraction patterns of $LuMnO_3$-A, $LuMnO_3$-B and $LuMnO_3$-C films.

compounds present in the substrate. The qualitative analysis of the EDS spectra reveals a 1:1 (Lu/Mn) molar ratio in agreement with the precursor solution composition.

Fig. 4 shows the scanning electron microscopy (SEM) plan-view images of the $LuMnO_3$-A, $LuMnO_3$-B and $LuMnO_3$-C films. $LuMnO_3$-A film exhibits a smooth surface (Fig. 4a), while the increase of the annealing temperature up to 800 °C results in an incipient grain growth, as observed in the $LuMnO_3$-B film (Fig. 4b). On the other hand, $LuMnO_3$-C film shows a well-defined structure with an average grain size of 170 nm. It is probably that the preferential grain growth, along with the substrate film stress induced at such high temperatures (850 °C), results in well-defined grain boundary, which is normally observed in stressed structures [19]. The grain growth evolution observed in the $LuMnO_3$ films plan-view images is consistent with the TG–DTA and X-ray results, which show the complete formation of a pure hexagonal $LuMnO_3$ perovskite phase with a (002) preferential orientation in the film annealed at 850 °C.

In order to determine the films surface roughness and to confirm the SEM surface morphology results, tapping mode atomic force microscopy images were carried out, as shown in Fig. 5. The films AFM images show an increase in the average film surface roughness as the annealing temperature increases, from 0.19 nm for $LuMnO_3$-A, through 0.47 nm for $LuMnO_3$-B and to 1.56 nm for $LuMnO_3$-C. This increase in the average surface roughness is visibly associated with the enhancement of the crystallization process and the formation of the hexagonal $LuMnO_3$ phase, as the annealing temperature increases. Whereas the AFM images of $LuMnO_3$-A and $LuMnO_3$-B films show the formation of an amorphous surface and an incipient grain growth, the AFM image of the $LuMnO_3$-C film reveals a well-defined structure with large grains and an average grain size of 170 nm, in good agreement with SEM analysis.

The analysis of the solution decomposition together with the structural and microstructural analysis reveal that the formation of a well-crystallized hexagonal phase in $LuMnO_3$ thin film is only achieved at annealing temperatures above to 800 °C. Consequently, the following section is only focused on the magnetic and dielectric characterization of the $LuMnO_3$-C film.

Table 1
Lattice parameters of $LuMnO_3$ ceramic, single crystal and thin film.

Samples	Space Group	Lattice parameter (a)	Lattice parameter (c)
$LuMnO_3$ ceramic	$P6_3cm$	6.0456(3) Å	11.3702(4) Å
$LuMnO_3$ single crystal	$P6_3cm$	6.038(1) Å	11.361(1) Å
$LuMnO_3$-C film	$P6_3cm$	6.006(3) Å	11.369(6) Å

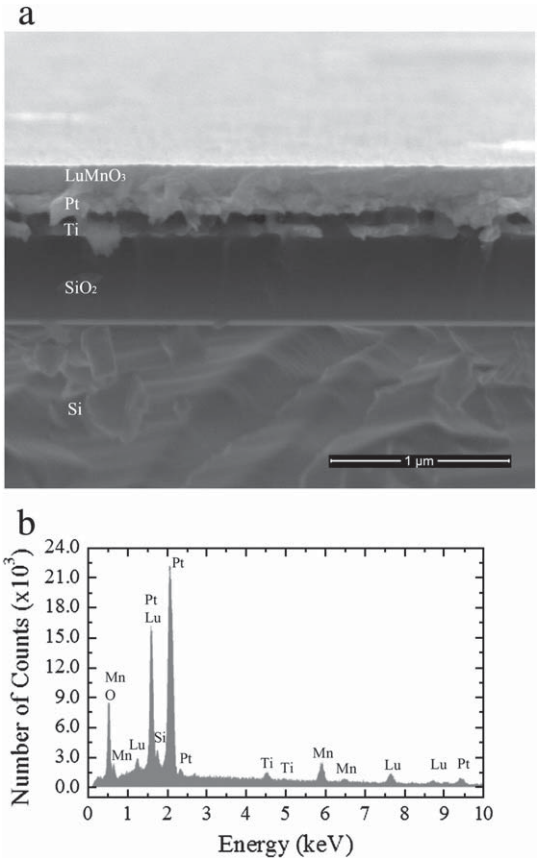

Fig. 3. a) Representative cross-section scanning electron microscopy image and b) EDS analysis of the $LuMnO_3$ thin films.

3.3. Magnetic and dielectric characterization

Fig. 6 shows temperature dependence of the specific induced magnetization of the $LuMnO_3$-C film, measured under an applied dc magnetic field of 10 mT, in a heating run after cooling the sample in zero-field (zero-field cooling conditions (ZFC)) and after cooling the sample under an applied magnetic field (field cooling conditions (FC)). Fig. 7 shows the H/M(T) curve, obtained from the ZFC curve. Above 120 K, the magnetization curves converge and follow a Curie–Weiss law, with a Curie temperature $\theta = -131.5$ K, and Curie constant $C = 3.33 \times 10^{-5}$ m^3K/mol. The obtained value for the effective paramagnetic moment is 4.55 μ_B, which is ~10% lower than the value reported by Tomuta et. al., for $LuMnO_3$ ceramics (4.78 μ_B) [14]. Both Curie temperature and Curie constant obtained do not also correspond to the ones reported for $LuMnO_3$ hexagonal ceramics. Moreover, the frustration coefficient value defined by the equation $(^{\theta}/_{T_N})$ is 1.5, which is in the same order of magnitude of the value reported for ceramics (5.8) [14]. It is clear that the frustration coefficient should be different for $LuMnO_3$ ceramics and films, which is mainly associated with the distortion of the oxygen by pyramidal structure provoked by the substrate clamping.

Below 100 K, the induced magnetization is strongly dependent on how the sample is cooled down. In fact, upon cooling the sample under an external magnetic field of 10 mT (FC conditions), a significant deviation from the ZFC curve is evidenced, reaching a 400% difference at 5 K, which is typically associated with a canted spin structure. Qualitatively, the magnetization curves obtained in our film are rather similar to the ones reported for ceramics, measured in the same conditions [20]. Furthermore, the magnitude of magnetization increase at the lowest temperature, both obtained in this work and reported for ceramics, are in excellent agreement [20]. These aspects enable us to conclude that the effect of the substrate on the magnetic

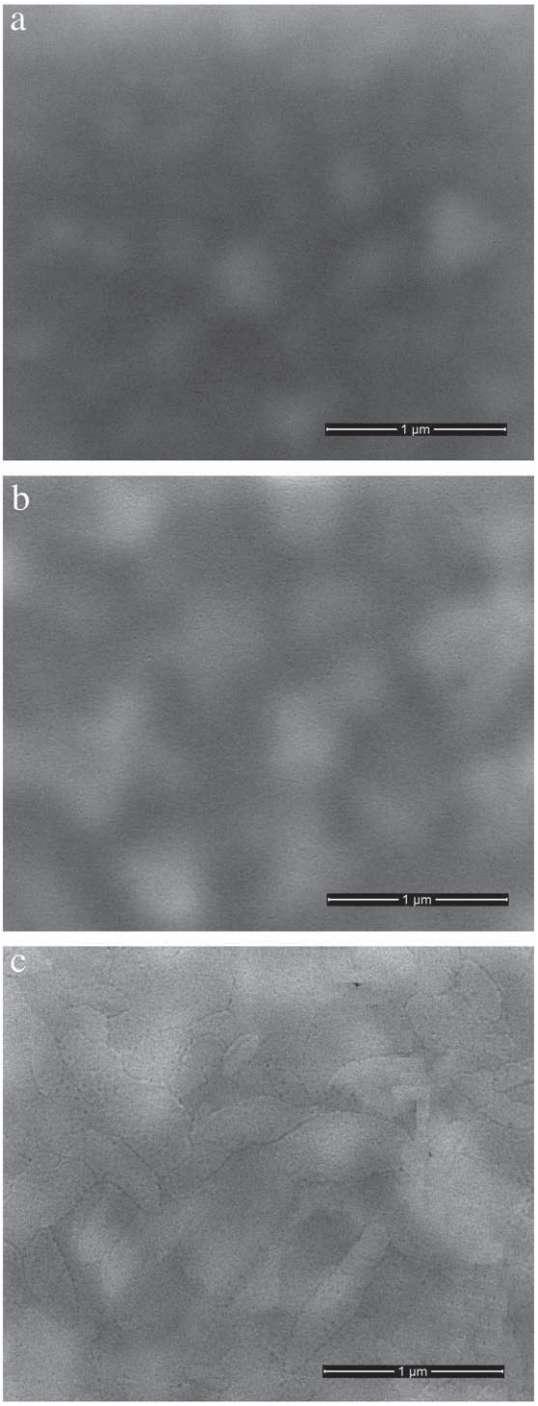

Fig. 4. Scanning electron microscopy images of: a) $LuMnO_3$-A, b) $LuMnO_3$-B and c) $LuMnO_3$-C thin films.

properties of the as-prepared films is apparently negligible on the magnetic properties of the $LuMnO_3$-C film.

On decreasing temperature, ZFC curve exhibits a step-like anomaly at $T_N = 85$ K, marking the phase transition from the paramagnetic to the incommensurate antiferromagnetic phase, which has been associated with the *c*-axis change [21,22]. On further cooling, the magnetization curve I exhibits another anomaly at 37 K, evidencing the transition to the E-type incommensurate antiferromagnetic phase, associated with the *in*-plane change of the *a* and *b* axes [21,22]. A tiny anomaly in the ZFC magnetization is observed at 12 K, which was also reported for ceramics. This anomaly has been assigned to a dramatic change of the Mn – O3 and Mn – O4 bond lengths [21].

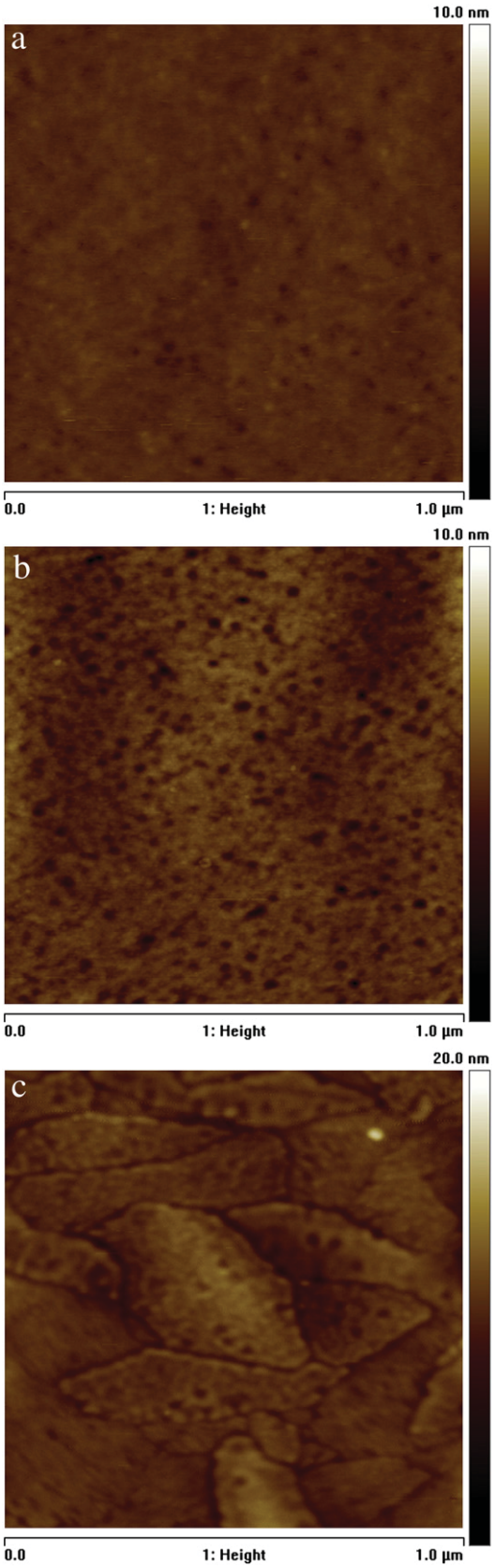

Fig. 5. Plan view AFM images of: a) $LuMnO_3$-A, b) $LuMnO_3$-B and c) $LuMnO_3$-C thin films.

Regarding the FC curve, an upward temperature shift of the step-like anomaly is observed. This effect of the cooling magnetic field on the Néel temperature was never observed in ceramic samples. It is

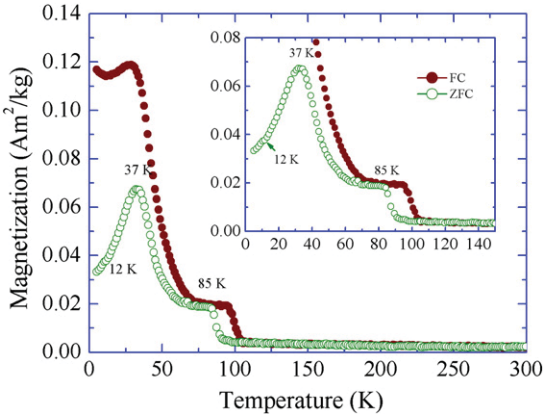

Fig. 6. Temperature dependence of the field cooling and zero field cooling magnetization for $LuMnO_3$-C thin film, carried out using a driving magnetic field of 10 mT.

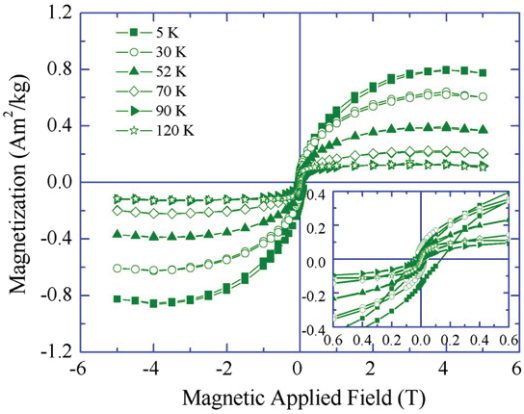

Fig. 8. Magnetic hysteresis loops of $LuMnO_3$-C film carried out at different temperatures.

worth noticing that the anomalous behavior observed in the ZFC curve at 37 K, takes place at 28 K in the FC curve, while a minimum value of the magnetization is detected at 12 K.

As it was referred to above, the increase of the magnetization below 100 K is consistent with the appearance of a ferromagnetic component in the low temperature magnetic phases of this compound, arising from the canted spin structure. We have ascertained this result by measuring M(H) for several fixed temperatures below 120 K, presented in Fig. 8. An apparent non-linear paramagnetic behavior is observed from 120 K down to 90 K. Non-centered hysteretic M(H) relations start to be visible below 90 K, typically observed in weak-ferromagnetic phases, where a preferential orientation is apparent. The remanent magnetization and the coercive field increase as the temperature decreases, as it can be seen in Fig. 9. The non-centered M(H) relations are consistent with the canted spin arrangement and with the preferential orientation of the as-processed films, along the [002] direction.

Fig. 10 shows the real (ε') and imaginary (ε'') parts of the dielectric permittivity as a function of the temperature for the $LuMnO_3$-C thin film, which were measured in heating run from 5 K up to 300 K over a frequency range from 1 kHz to 1 MHz, using a driving signal of 0.1 V. ε'(T) increases as the temperature increases up to 85 K, showing a frequency that is almost-independent dielectric constant. However, above 85 K two shoulders appear, which are more evident at higher frequencies (i.e., 1 MHz). On the other hand, ε''(T) shows two frequency dependent anomalies. These anomalies converge to a broader complex anomaly at 1 kHz. Moreover, below 85 K ε''(T) slightly decreases as the temperature decreases, showing also a magnitude drop as the frequency falls.

Similar low temperature ε' frequency dependence was already found on $LuMnO_3$ ceramics [20]. However, the higher temperature ε' frequency dependence shoulder has never been reported in this material. Nevertheless, it is evident that this high temperature shoulder is not associated with the ferroelectric–paraelectric phase transition, which occurs at higher temperatures. In fact, a transition to the ferroelectric phase at 740 K was reported in ceramic and single crystal of lutetium manganite [20,23]. Moreover, since $LuMnO_3$ ceramics do not show any relaxation process in the 100 K–300 K temperature range, the complex frequency behavior of the dielectric permittivity observed in our $LuMnO_3$-C film could be associated with relaxation processes arising from the interfaces film/electrodes. In order to determine the driving forces associated with them, further experimental work is still needed.

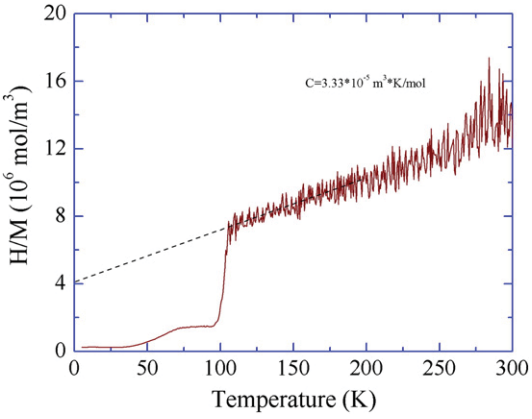

Fig. 7. Temperature dependence of inverse of the susceptibility and Curie–Weiss fitting for $LuMnO_3$-C film.

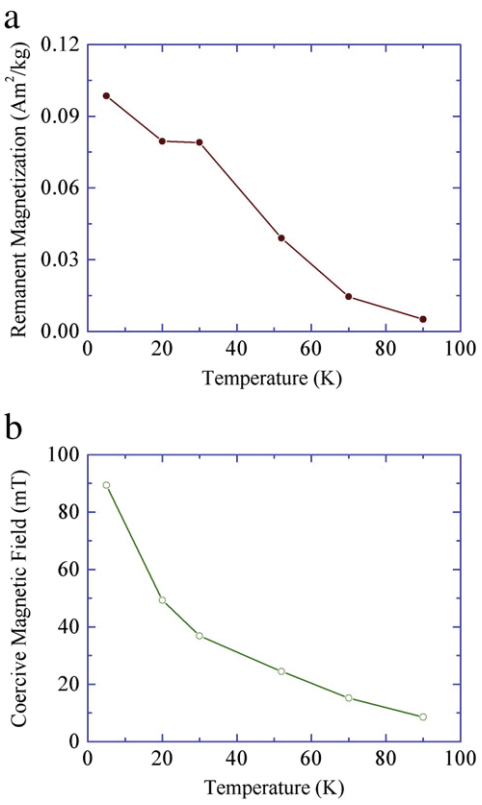

Fig. 9. Temperature dependence of: a) remanent magnetization and b) coercive field obtained from the experimental hysteresis loops data of the $LuMnO_3$-C film.

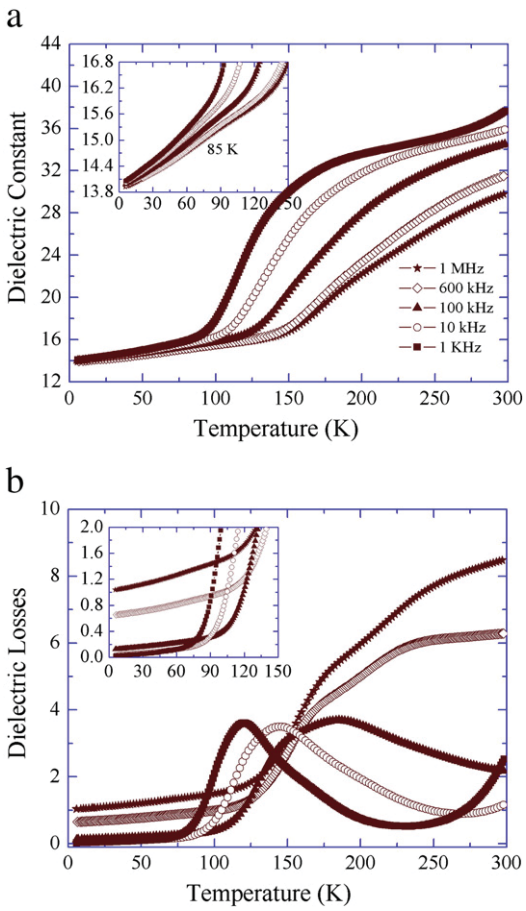

Fig. 10. Temperature dependences of real and imaginary parts of the dielectric permittivity for the $LuMnO_3$-C thin films, carried out at several frequencies.

4. Conclusions

$LuMnO_3$ thin films were prepared by chemical solution deposition and deposited on $Pt/TiO_2/SiO_2/Si$ substrate by a spin-coating method. The films were annealed from 750 °C up to 850 °C based on the TG and DTA $LuMnO_3$ solution decomposition process and phase formation. X-ray diffraction analysis shows the formation of a pure $LuMnO_3$ hexagonal phase at 800 °C and 850 °C, while SEM morphology analysis reveals the enhancement of the $LuMnO_3$ film crystallization as the annealing temperature increases.

The study of the magnetic properties at low temperature in lutetium manganite films yields magnetic transitions, which are consistent with those reported for the corresponding ceramics and single crystals. Above 120 K, M(T) follows a Curie–Weiss law, with $\theta = -131.5$ K, and $C = 3.33\times10^{-5}$ m^3K/mol. Furthermore, an effective paramagnetic moment of 4.55 μ_b is obtained. It is worth noting that the values referred to above do not match those reported for ceramics.

The significant difference between M(T) measured under ZFC and FC conditions reaching a 400% difference at 5 K reveals the emergence of a canted spin structure. Non-centered M(H) relations are also consistent with the canted spin arrangement referred to above, but still with the preferential orientation of the as-processed films along the [002] direction.

Since a qualitatively similarity exists between M(T) obtained for $LuMnO_3$ films and ceramics, the effect of the substrate on the magnetic properties of the as-prepared films is apparently minor.

Dielectric measurements of the $LuMnO_3$ thin film annealed at 850 °C reveal the existence of a complex frequency behavior of the dielectric permittivity, which could be associated with relaxation processes arising from the interfaces film/electrodes.

Acknowledgment

Authors thank Fundação para a Ciência e Tecnologia (FCT) for the financial support (PTDC/CTM/099415/2008). Y. Romaguera also thanks the financial support by the Programme Alβan (The European Union Programme of High Level Scholarships for Latin America, scholarship no. E07D401169CU).

References

[1] H.Y. Hwang, S.W. Cheong, P.G. Radaelli, M. Marezio, B. Batlogg, Phys. Rev. Lett. 75 (1995) 914.
[2] N. Fujimura, T. Ishida, T. Yoshimura, T. Ito, Appl. Phys. Lett. 69 (1996) 1011.
[3] D. Ito, N. Fujimura, T. Yoshimura, T. Ito, J. Appl. Phys. 93 (2003) 5563.
[4] W. Prellier, M.P. Singh, P. Murugavel, J. Phys. Condens. Matter 17 (2005) R803.
[5] W.S. Choi, D.G. Kim, S.S.A. Seo, S.J. Moon, D. Lee, J.H. Lee, H.S. Lee, D.Y. Cho, Y.S. Lee, P. Murugavel, J. Yu, T.W. Noh, Phys. Rev. B 77 (2008) 045137.
[6] G. Lalitha, P.V. Reddy, J. Magn. Magn. Mater. 320 (2008) 754.
[7] A. Filippetti, N.A. Hill, J. Magn. Magn. Mater. 236 (2001) 176.
[8] Z.J. Huang, Y. Cao, Y.Y. Sun, Y.Y. Xue, C.W. Chu, Phys. Rev. B 56 (1997) 2623.
[9] D. Rubi, S. Venkatesan, B.J. Kooi, J.Th.M. De Hosson, T.T.M. Palstra, B. Noheda, Phys. Rev. B 78 (2008) 020408.
[10] N. Fujimura, T. Takahashi, T. Yoshimura, A. Ashida, J. Appl. Phys. 101 (2007) 09M107.
[11] T. Katsufuji, M. Masaki, A. Machida, M. Moritomo, K. Kato, E. Nishibori, M. Takata, M. Sakata, K. Ohoyama, K. Kitazawa, H. Takagi, Phys. Rev. B 66 (2002) 134434.
[12] B.B. Van Aken, T.T.M. Palstra, A. Filippetti, N.A. Spaldin, Nat. Mater. 3 (2004) 164.
[13] A.B. Souchkov, J.R. Simpson, M. Quijada, H. Ishibashi, N. Hur, J.S. Ahn, S.W. Cheong, A.J. Millis, H.D. Drew, Phys. Rev. Lett. 91 (2000) 027203.
[14] D.G. Tomuta, S. Ramakrishnan, G.J. Nieuwenhuys, J.A. Mydosh, J. Phys. Condens. Matter 13 (2001) 4543.
[15] B.B. van Aken, A. Meetsma, T.T.M. Palstra, Acta Crystallogr. E 57 (2001) i101.
[16] N. Imamura, M. Karppinen, H. Fjellvåg, H. Yamauchi, Solid State Commun. 140 (2006) 386.
[17] Y.R. Barcelay, J.A. Moreira, G.G. Aguilar, A. Almeida, J.P. Araujo, J.P. de la Cruz, J. Electroceram. 26 (2011) 44.
[18] K.T. Kim, C.I. Kim, J. Eur. Ceram. Soc. 24 (2004) 2613.
[19] M.W. Barsoum, Fundamental of Ceramics, IOP Publishing Ltd., Bristol, UK, 2003.
[20] A. Ghosh, J.R. Sahu, S.V. Bhat, C.N.R. Rao, Solid State Sci. 11 (2009) 1639.
[21] J.S. Zhou, J.B. Goodenough, J.M. Gallardo-Amores, E. Morán, M.A. Alario-Franco, R. Caudillo, Phys. Rev. B 74 (2006) 014422.
[22] T. Goto, T. Kimura, G. Lawes, A.P. Ramirez, Y. Tokura, Phys. Rev. B 92 (2004) 257201.
[23] L.E. Cross, Ferroelectrics 76 (1987) 241.